Multi-axial DNA origami force spectroscopy reveals hidden dynamics of Holliday junctions

Gde Bimananda Mahardika Wisna[a,b,c,1], **Ayush Saurabh**[a,d], **Deepak Karna**[b], **Ranjan Sasmal**[b], **Prathamesh Chopade**[b], **Steve Pressé**[a,c,d], **and Rizal F. Hariadi**[a,b,c,1]

[a]Department of Physics, Arizona State University, Tempe, Arizona, USA.; [c]Center for Molecular Design and Biomimetics at the Biodesign Institute, Arizona State University, Tempe, Arizona, USA.; [b]School of Molecular Sciences, Arizona State University, Tempe, Arizona, USA.; [d]Center for Biological Physics, Arizona State University, Tempe, Arizona, USA.

[1]To whom correspondence should be addressed. E-mail: {gwisna,rhariadi}@asu.edu
This manuscript was compiled on September 24, 2025

Abstract

Biomolecules in living cells experience complex multi-directional mechanical forces that regulate their structure, dynamics, and function. However, most single-molecule techniques primarily exert force along a single axis, thereby failing to emulate the mechanical cellular environment. Here, we present Multi-Axial Entropic Spring Tweezer along Rigid DNA Origami (MAESTRO), a molecular platform that applies up to 9 pN forces from up to four directions simultaneously using programmable ssDNA entropic springs anchored to a rigid DNA origami scaffold. Combining MAESTRO, single-molecule Förster resonance energy transfer (smFRET), and Bayesian non-parametric FRET (BNP-FRET) enables a high-throughput study of biomolecules under different complexities of multi-axial tension forces. We applied MAESTRO to Holliday junctions (HJs), four-way DNA intermediates that experience multi-directional tension during homologous recombination. Counterintuitively, we discovered $\geq 5\times$ slower kinetics of the HJ conformations under multi-axial tension than under tension-free conditions, enabling direct observations of previously hidden HJ conformational intermediates. Most remarkably, we discovered that multi-axial tension restores quasi-ergodicity to HJ dynamics by overcoming the rugged energy landscape, enabling direct observation of kinetic class interconversion within individual molecules—a phenomenon previously thought impossible—that reveals the conformational landscape is far more interconnected than understood and fundamentally challenges existing models. Furthermore, we demonstrated that this conformational control regulates T7 endonuclease I cleavage site selection, directly linking mechanical environments and molecular mechanics to enzymatic function. By overcoming single-axis limitations, MAESTRO opens new frontiers in molecular mechanobiology, revealing how physiologically relevant multi-directional forces access expanded conformational landscapes and can serve as master regulators for biomolecular function through mechanisms inaccessible to conventional single-axis approaches.

Key words: single-molecule dynamics, DNA origami, force spectroscopy, multi-axial tension, Holliday junction, single-molecule FRET, mechanobiology, enzyme regulation, ergodicity.

Introduction

Mechanical forces on the order of pN acting at the single-molecule level have a profound effect on biomolecular function by inducing nanometer-scale structural changes. Mechanical forces arise through either active mechanisms, where biomolecules convert chemical energy into mechanical work,

or passive mechanisms, where biomolecules experience pulling and stretching from their surroundings. The strengths of this mechanical work are comparable to the thermal energy scale of $k_BT \sim 4.2$ pN.nm, suggesting that multi-axial forces broadly influence biomolecular processes.[1]

To investigate the mechanics at the single-molecule level, a variety of revolutionary force spectroscopy tools have been utilized, including optical[2] and magnetic tweezers[3], atomic force microscopy[4], centrifugal force spectroscopy[5], DNA-based tension probes[6–9], and a DNA nanoscopic force clamp[10,11], often in tandem with single-molecule fluorescence microscopy.[12] These approaches have successfully quantified the mechanical energy generated by the rotary motor F1-ATPase under specified loads[13], identified the stall force of motor proteins such as myosins and kinesins[14,15], measured the stalling tension in T7-DNA polymerase[16], investigated stacking forces among DNA bases[17], observed conformational changes of DNA Holliday junctions under tension[18], analyzed the activation of different mechanosensitive membrane proteins[6–9], and explored the energetics involved in protein folding and unfolding.[19,20] These techniques successfully address numerous aspects of single-molecule biophysics, achieving high precision over a diverse range of tensions, as seen with atomic force microscopy and magnetic tweezers, and providing high-throughput capabilities, as demonstrated by magnetic tweezers, centrifugal force spectroscopy, DNA origami-based spectroscopy, and DNA-based tension probes. However, they are limited to applying forces in a single direction due to challenges related to alignment and stability, the complexity of force calibration and measurement, and the difficulties in incorporating multiple tether or anchor points without inducing twisting or buckling.[21–23]

Multi-directional forces are ubiquitous in cellular mechanobiology, where biomolecules experience simultaneous tension from multiple sources. Focal adhesion proteins like integrin experience forces from both extracellular matrix attachment and intracellular cytoskeletal networks, creating multi-directional stress patterns essential for cellular mechanosensing.[24,25] Similarly, chromatin-associated proteins experience simultaneous forces from nucleosome interactions, transcriptional machinery, and DNA repair complexes during processes like homologous recombination.[26] Despite the biological relevance, methods to exert multi-axial tension and simultaneously monitor biomolecular functions have yet to be developed, limiting our understanding of how mechanical forces regulate biomolecular function in living cells.

To address this limitation, we leverage DNA origami[27,28] and entropic springs[11,29] to apply multi-axial tension forces to biomolecules. With DNA origami, any rigid 3D shape can be realized through the folding of a long single-stranded DNA (ssDNA) scaffold with hundreds of short ssDNA staple strands via Watson-Crick base-pairing. We choose a 3D DNA origami ring as a rigid platform with circular symmetry[30] to pattern several ssDNAs with specific lengths spanning the diameter of the origami structure. These ssDNA strands act as entropic springs, each generates a defined tension in the range of $0-9$ pN along the spring due to the thermal fluctuations.[11,29]

To investigate the effects of physiological multi-axial forces, we chose the Holliday junction (HJ) as our model system. HJs form as central intermediates during homologous recombination, the primary mechanism for repairing DNA double-strand breaks caused by ionizing radiation or replication errors[31–36] (Fig.1(a)). During this repair process, DNA strands undergo chromatin remodeling while remaining bound to histones, creating multi-directional tension environments where each of the junction's 4 arms experiences independent forces from chromatin compaction, protein binding, and branch migration processes. We hypothesize that these multi-axial forces influence how resolvases bind to HJs and bias cleavage patterns toward crossover or non-crossover repair products, potentially affecting genetic outcomes during DNA repair. Furthermore, HJs conformational flexibility and force sensitivity[18] make them ideal targets for investigating how physiologically relevant multi-directional forces regulate biomolecular function.

Our experiments using MAESTRO reveal, for the first time, HJ dynamics under multi-axial tension. We find these dynamics to be kinetically heterogeneous, with various combinations of fast and slow transition rates for both high and low FRET conformations. Contrary to the common expectation that forces increase reaction rates, we discovered that multi-axial tension dramatically slows the junction's isomerization kinetics by 5×. This kinetic trapping allowed us to directly observe previously unseen,

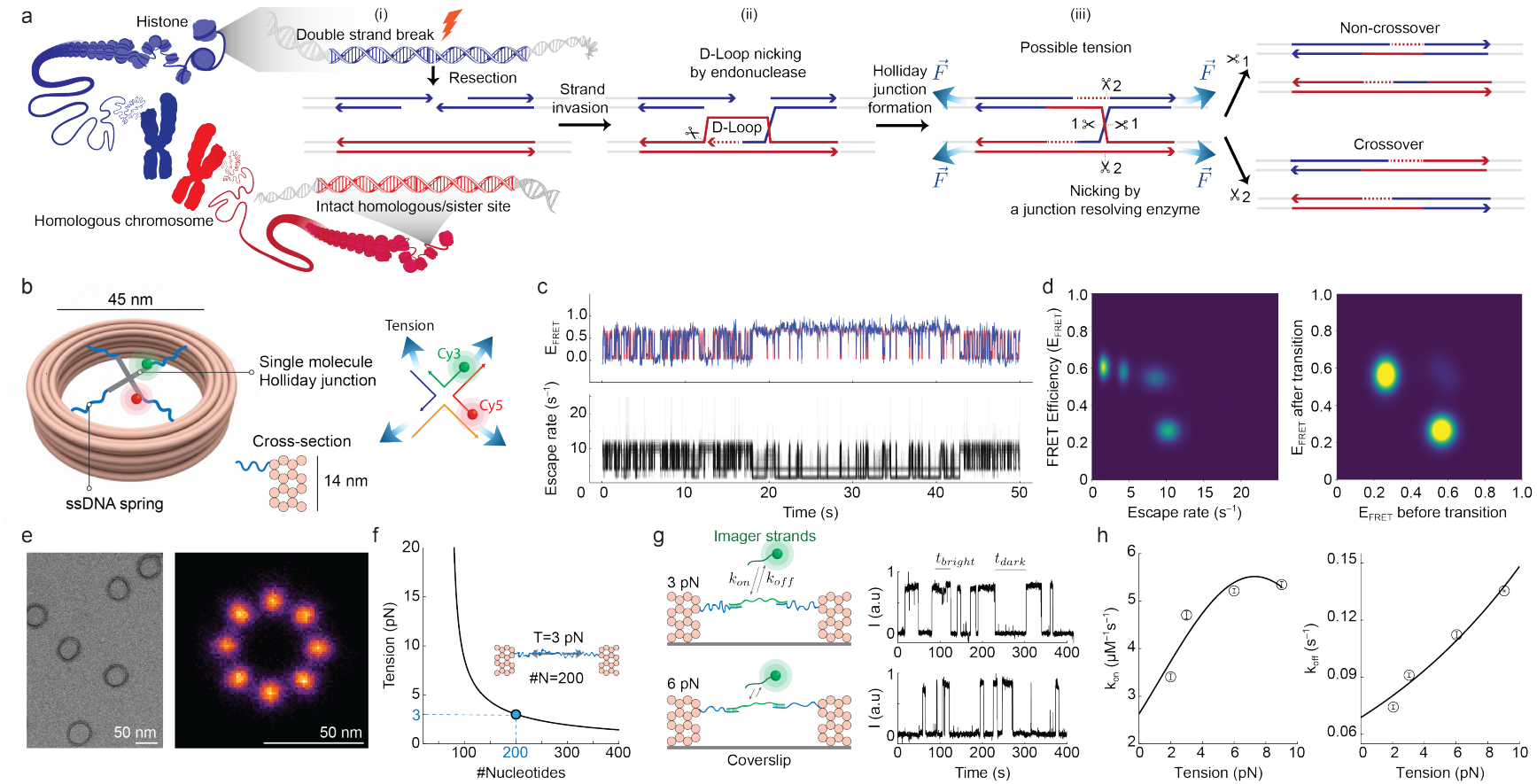

Fig. 1 MAESTRO platform design, validation, and force characterization. (**a**) Chromatin remodeling enabled formation of Holliday junction during homologous recombination showing double-strand break, D-loop invasion under multi-axial tension. (**b**) MAESTRO schematic showing HJ under controlled multi-axial tension via entropic ssDNA springs. (**c**) Representative smFRET trajectory with Bayesian non-parametric FRET (BNP-FRET) analysis showing HJ dynamics and escape rates (sum of transition rates out of each state). (**d**) Escape rate and transition density heatmaps (N=1000 samples). (**e**) Structural validation by negative stain-TEM (left) and DNA-PAINT super-resolution imaging (right, N=412). PAINT shows the possible anchoring points for entropic springs. (**f**) Force-extension relationship based on the modified FJC model. (**g**) DNA hybridization kinetics under tension showing bright/dark time analysis. (**h**) Tension-dependent association and dissociation rates with fitted curves. Error bars: SD from bootstrapping.

short-lived intermediate conformations. Furthermore, we found that multi-axial tension facilitates the interconversion between distinct kinetic behaviors, a phenomenon not observed under single-axial force. These findings fundamentally challenge the conventional understanding of how mechanical forces regulate molecular dynamics, revealing a hidden landscape that only emerges under multi-axial tension.

Results

MAESTRO recreates a physiological tension environment where biomolecules experience tension from multiple sources, overcoming the single-axis limitation of force spectroscopy. We designed MAESTRO as a molecular platform capable of applying programmable multi-axial pN forces at the single-molecule level, overcoming the fundamental limitation that has constrained force spectroscopy to single-axis applications. The architecture of MAESTRO comprises a rigid DNA origami ring with diameter ∼45 nm and a height of ∼14 nm, constructed from 16 curved double-stranded DNA (dsDNA) (Fig. 1(b)).[30] Its circular symmetry enables the anchoring of multiple single-stranded DNA (ssDNA) entropic springs along the inner sidewalls, which apply single- or multi-axial tension forces to the HJ while maintaining structural rigidity for precise control (Figs. 1(b), S1 and Table S1). HJs exist in dynamic equilibrium between 2 stacked isomers, namely Iso-I and Iso-II, that differ in which pairs of DNA arms stack together, with transitions mediated by transient open conformations in which all four arms are unstacked. We investigated the dynamics of HJ (Table S2 for the complete DNA sequences) under various tension configurations using single-molecule Förster Resonance Energy Transfer (smFRET), where the junctions transition between 2 stacked isomers (Iso-I and Iso-II) with distinct FRET efficiencies (E_{FRET}) of ∼0.6 and ∼0.25, respectively (Fig. 1(c and d)).

Our smFRET experiments revealed a wide range of kinetic behaviors among the HJs under tension, implying that each smFRET trajectory can have a distinct set of transition rates between the HJ conformations. Consequently, to observe previously unseen dynamics, we avoid fixing the number of states in advance for the entire population when analyzing our smFRET datasets, as is commonly performed when using traditional hidden Markov model (HMM)-based techniques.[37] Therefore, we chose to use Bayesian non-parametric FRET (BNP-FRET)[37,38] to analyze the smFRET trajectories and extract key kinetic parameters. This method implements an infinite-dimensional HMM and uses Markov chain Monte Carlo (MCMC) techniques to generate samples for the number of states, state trajectories, transition rates, and FRET efficiencies. Furthermore, BNP-FRET uses an accurate noise model for our sCMOS camera and incorporates pixel-by-pixel camera calibration maps to optimally recover the signal from the noisy smFRET data. Finally, the BNP-FRET samples can then be collected together to generate heatmaps for escape rates λ (sum of all transition rates out of a given state) as well as transition densities (Fig. 1(c and d)), and estimate the uncertainties.

The rigidity and addressability of MAESTRO enable precise multi-directional force application. We employed negative-stain transmission electron microscopy (ns-TEM) to validate that MAESTRO retained its programmed rigid and circular structure (Fig. 1(e)). This rigidity is critical for reliably anchoring entropic ssDNA springs and ensuring accurate tension force estimates based on the modified freely jointed chain (FJC) model.[11,29] Additionally, we performed DNA-PAINT super-resolution imaging[39] to demonstrate the addressability of 8 sites on the inner sidewall of MAESTRO (Tables S1 and S3) . Fig. 1(e) shows eight specific attachment sites where ssDNA springs can be precisely anchored to MAESTRO and meet at a target molecule at the center of MAESTRO (Fig. S2). The tension along the ssDNA spring can be tuned by varying the contour length using the modified FJC model (Fig. 1(f); Methods). For example, a 200 nt ssDNA spring that spans the inner diameter of MAESTRO (Fig. 1(f) inset) produces 3 pN. This exquisite positional control provides the necessary foundation for applying well-defined magnitudes and net directions to pN-scale forces.

Force-dependent DNA hybridization kinetics validates the precision of MAESTRO across the physiologically relevant 0–9 pN range. To quantitatively validate the ability of MAESTRO to exert

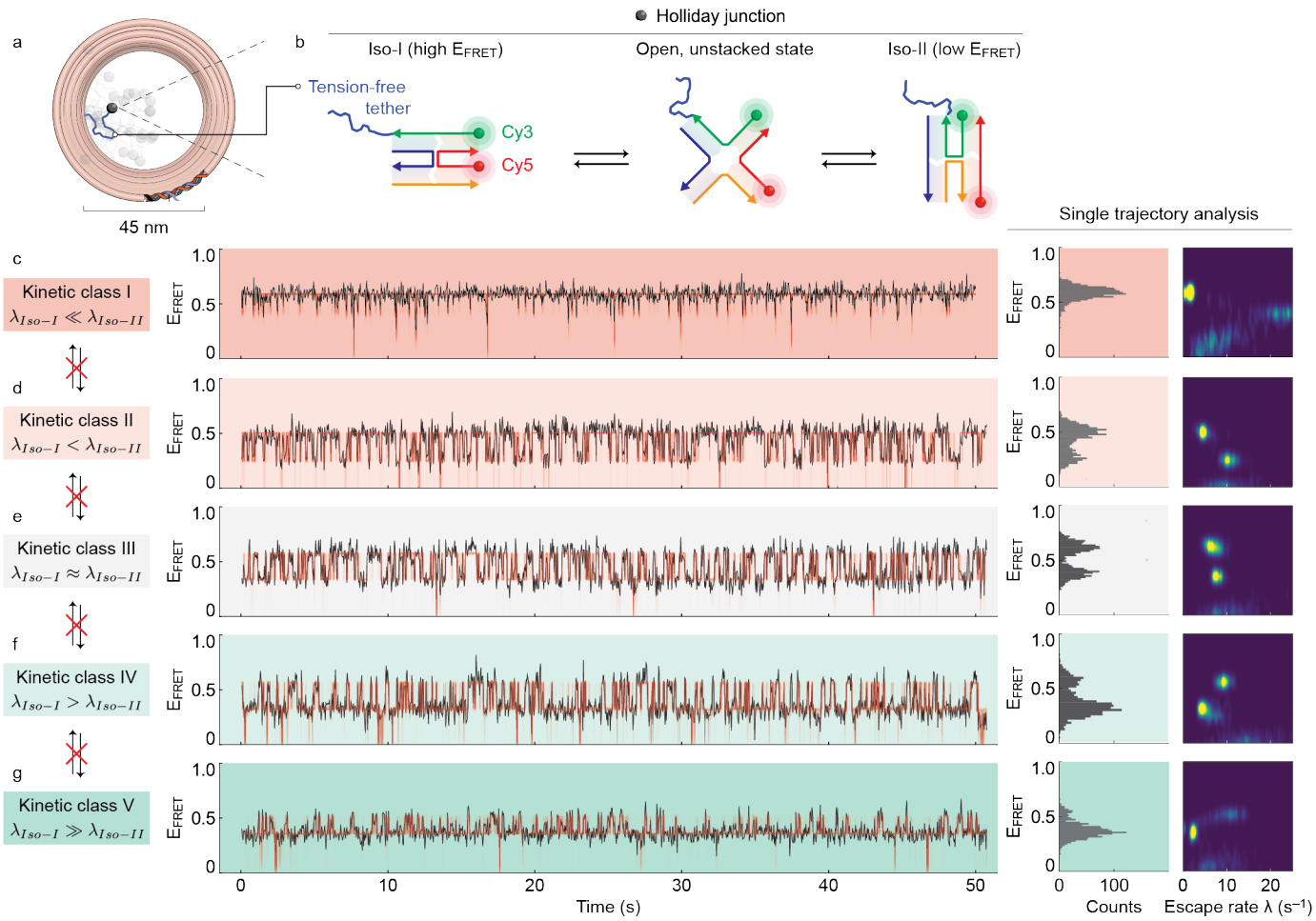

Fig. 2 Five kinetic classes of Holliday junction dynamics characterized by FRET efficiency. (**a**) MAESTRO platform with HJ tethered (black sphere) to a 0 pN entropic spring (blue). Transparent spheres illustrate HJ spatial dynamics. (**b**) HJ conformational switching between 2 states (Iso-I: $E_{FRET} \sim 0.6$; Iso-II: $E_{FRET} \sim 0.25$) monitored through a FRET pair. (**c-g**) Five kinetic classes with distinct HJ dynamics were observed in different HJ molecules of the same sequence within a single field of view (left panels). (Left) Each row shows a representative 50-sec smFRET trajectory (black) and its corresponding BNP-FRET trajectory (red). (Middle) Histograms of E_{FRET} for different kinetic classes. (Right) Escape rate heatmaps define the characteristic features of each kinetic class. The color scheme for kinetic classes in (**c–g**) is consistent with Fig. 3.

precise tension on target molecules, we developed an assay grounded in the tension-dependent hybridization kinetics of complementary short single-stranded DNAs. One strand (the docking strand) is held under a defined tension on the MAESTRO, whereas the complementary strand freely diffuses until hybridization under tension occurs (Fig. 1(g), Tables S1 and S4). Kinetic measurements were performed using DNA-PAINT super-resolution imaging. By varying the lengths of the ssDNA springs, we generated predicted tension forces of 2, 3, 6, and 9 pN along the docking strands. The DNA-PAINT under tension assay confirmed that MAESTRO applies precise and predictable pN-scale forces. We observed that both the association (k_{on}) and dissociation (k_{off}) rates of a short DNA duplex were systematically increased with the applied tension (Figs. 1(h) and S3). These trends, including the asymptotic plateau of k_{on} and the exponential growth of k_{off}, are in agreement with previous studies on force-dependent hybridization kinetics (Methods).[40] Furthermore, our extrapolated rate at 0 pN force ($k_{\text{on}}(0) = 2.63$ μ/M/sec) closely matches the literature value for this specific DNA sequence,[41] providing independent confirmation of our force calibration.

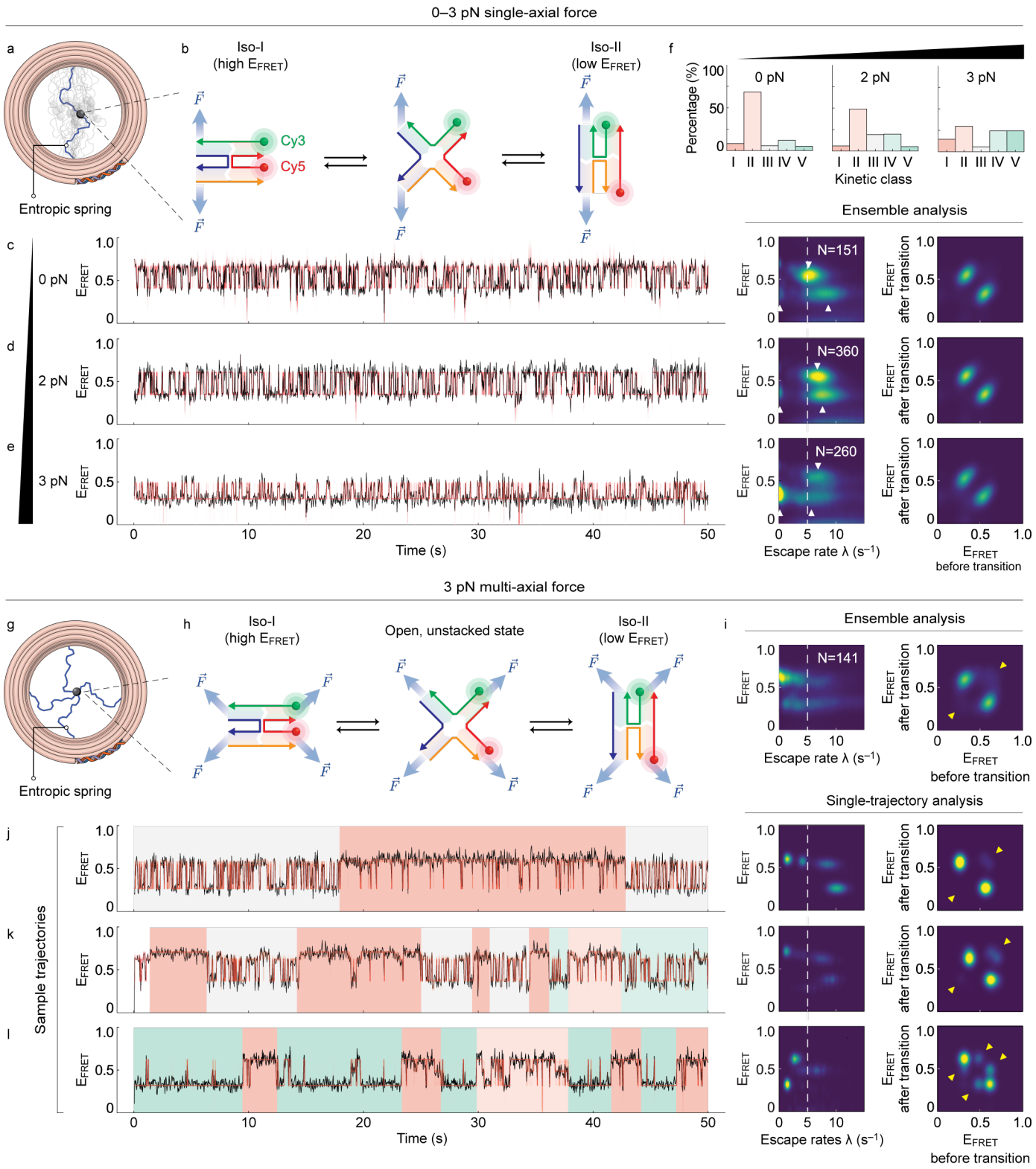

HJ dynamics reveal ergodicity breaking through heterogeneity across 5 non-interconverting kinetic classes. With MAESTRO's force accuracy established, we characterized the baseline HJ dynamics under tension-free conditions to provide a foundation for detecting multi-axial force effects. To achieve a tension-free condition, each HJ was connected to a MAESTRO by a single ssDNA tether (Fig. 2(a)), allowing the observation of intrinsic conformational dynamics without applied mechanical stress. HJs

Fig. 3 (Previous page) Multi-axial forces reveal hidden dynamics and enable kinetic class switching. (**a,b**) Single-axial tension setup: Two HJ arms are attached to a pair of entropic springs (blue) spanning the MAESTRO diameter and anchored at diametrically opposite attachment sites. The force direction is indicated by blue arrows. (**c–e**) smFRET trajectories (black) and their corresponding BNP-FRET trajectories (red) demonstrate progressive shifts in class populations and dynamics as the tension increases from 0 to 3 pN (N = 151–360 for each condition), with corresponding escape rate heatmaps. (**f**) Ensemble analysis showing the kinetic class population distributions at the denoted applied tensions. (**g,h**) Multi-axial configuration: Each of the four HJ arms is coupled to its own entropic spring. A four-way tension of 3 pN was applied along the orthogonal axes as the HJ was pulled outward from the center. (**i**) Ensemble heatmaps of escape rates and transition E_{FRET}. (**j–l**) FRET trajectories (black) and their corresponding BNP-FRET trajectories (red) show dramatic class switching within 50-sec observation windows (N = 141). Colored background regions highlight the periods of different kinetic classes. White dashed line indicates the escape rate of Iso-I under 0 pN tension. White arrows indicate the escape rates of Iso-I or Iso-II which shows the effect of single-axial tension on the escape rates, and yellow arrows highlight previously undetected intermediate states. The color scheme for kinetic classes in panels (**f**) and (**i–l**) is consistent with Fig. 2.

transition between two stacked isomers (Iso-I and Iso-II) through transient open states (Figs. 2(b)), displaying kinetic heterogeneity that we classified into five distinct classes based on escape rate ratios (Figs. 2(c–g), S4). These classes ranged from kinetically trapped (Classes I and V, with escape rates $<1\ s^{-1}$) to dynamically balanced (Class III, with comparable escape rates $\sim 5\ s^{-1}$), reflecting the complex energy landscape governing the HJ conformational dynamics. Distinct kinetic signatures are evident in both the escape rate distributions and transition density heatmaps, where trapped classes show narrow, single-peaked histograms, whereas dynamic classes exhibit broader, multi-peaked distributions, reflecting more frequent state sampling. Our classification reproduces the kinetic heterogeneity and non-interconverting behavior of surface-immobilized HJs without MAESTRO, validating that MAESTRO preserves the intrinsic HJ dynamics.[42] Crucially, each HJ molecule remained within its kinetic class throughout our 50-sec observation window. The 50-sec exposure time is $>100\times$ longer than the inverse of individual conformational escape rates in the escape rate heatmaps in Fig. 2. The absence of kinetic class interconversion underscores the non-ergodic nature of HJs under 0 pN, where kinetic class interconversion timescales far exceed the observation time, a kinetic constraint that would prove critical for detecting the profound effects of multi-axial forces in Fig. 3.

Single-axial forces create a static kinetic landscape that traps HJ conformations along the direction of the applied tension. Single-axial tension acted as a predictable kinetic clamp, stabilizing the HJ conformation aligned with the force vector in agreement with established mechanical models. Tension along the y-axis (Figs. 3(a and b)) favored the Iso-II conformation (Figs. 3(c–e)) and S5). The observed trends agree with earlier findings from optical tweezers experiments on HJs under tension[18] and DNA origami-based force using entropic springs.[11] Together, these findings confirm that MAESTRO effectively applies mechanical tension to HJ molecules, reshaping their dynamical behavior. This stabilization arises from a force-induced tilt in the free-energy landscape. While still obeying the principle of detailed balance, this tilt in the energy landscape increased the escape rate for the conformation orthogonal to the imposed tilt while significantly slowing the escape rate from the conformation aligned to the applied force. Consequently, the force-aligned conformation is effectively trapped. This kinetic trapping was confirmed by a progressive redistribution of kinetic classes under increasing tension, which favored the kinetically trapped Class V (Fig. 3(f)) while depleting more dynamic populations (Class II; Fig. 3(f)). Notably, these kinetic classes remained static for individual molecules, with no interconversion observed within our experimental timescale. While these findings confirmed the predictions of established mechanical models for simple single-axial force geometries, there may be some limitations of these models in the face of the complex dynamics induced by multi-axial tension.

Multi-axial tension slows HJ kinetics. We further explored the dynamics of HJs under multi-axial tension using 4-way tension (Figs. 3(g and h), S6, and S7). Despite the mechanical complexity of applying tension in four directions simultaneously, the ensemble transition heatmaps still show two major hotspots (Fig. 3(i)), while revealing previously hidden states as dimmer hotspots (yellow arrows; Fig. 3(i)). In stark contrast to conventional models predicting that the applied force increases the rate of conformational transitions, multi-axial tension drove a dramatic, >5× slowing of HJ kinetics (Fig. 3(i)). Analysis of escape rates revealed a high density of values that were >5× slower (Fig. 3(i)) than those observed under the 0 pN condition (white dashed line, Fig. 3(c) compared with Fig. 3(c and i–ℓ). This kinetic slowdown of both $\lambda_{\text{Iso-I}}$ and $\lambda_{\text{Iso-II}}$ are prominently visible in the escape rate heatmaps (Fig. 3(j–ℓ)), leading us to hypothesize the stabilization of intermediate open, unstacked conformations. These conformational states are normally too transient to be observed in the absence of multi-axial tension with our 10–25 ms exposure time. This hypothesized stabilization enables previously inaccessible levels of conformational connectivity.

Multi-axial tension restores quasi-ergodicity, transforming the static and rugged kinetic landscape into a dynamic and interconnected network. Most remarkably, 4-way tension induced quasi-ergodic sampling by collapsing the static kinetic classes observed under either 0 pN (Figs. 2 and 3(c)) or simpler single-axial tension (Fig. 3(a–e)), enabling many individual molecules to interconvert between the kinetic classes multiple times over a 50-sec observation window (Fig. 3(j–ℓ)). Additional examples of the four-way tension dynamics which show kinetic class interconversion are shown in Fig. S7. While the transition density heatmap confirms that most transitions occur between the two main states, the corresponding escape rate trajectory and heatmap reveal multiple degenerate states with distinct escape rates. The quasi-ergodicity emerged because multi-axial tension transformed the kinetic landscape from a set of discrete, isolated pathways into a dynamic, interconnected network, enabling individual molecules to explore previously inaccessible regions of the conformational space. This is a significant difference over the previous work[42], which could only induce a single interconversion event by chemically stripping Mg^{2+} from the junction region to reset the HJs and then reintroducing Mg^{2+} ions. In contrast, our platform achieved multiple spontaneous stochastic interconversions in equilibrium buffer conditions containing 12.5 mM Mg^{2+}, revealing that multi-axial forces expand access to previously hidden kinetic pathways. This suggests that the underlying conformational landscape is far more complex than that revealed by single-directional perturbations. Three-way tension also induced kinetic class interconversion, albeit less common than under 4-way tension (Fig. S5 and S8), confirming that multi-axial forces generally enable dynamic exploration of the energy landscape.

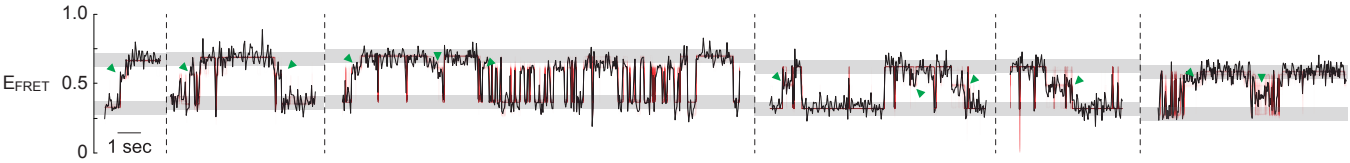

Fig. 4 Direct observation of stabilized transition states under 4-way tension. Selected regions of multiple smFRET (black) and their corresponding BNP-FRET trajectories (red) around interconversion events. Green arrows indicate observed transition states stabilized under multi-axial tension, with lifetimes extended from <80 ms to 1 s. Grey-shaded bands with height 0.1 E_{FRET} highlight the ranges corresponding to canonical Iso-I and Iso-II conformations; transition states fall outside these ranges, representing the open, unstacked conformation that mediates kinetic class interconversion.

Multi-axial tension stabilizes transition states, enabling direct observation of open conformations. The dramatic kinetic slowing observed under multi-axial tension suggests the stabilization of previously undetectable transition states. Using the BNP-FRET framework to analyze the regions surrounding interconversion events, we directly observed intermediate FRET states between the canonical Iso-I and Iso-II conformations (green arrows in Fig. 4). These states represent the open, unstacked conformation that

mediates isomer interconversion, a state that typically persists for less than 80 ms under high-divalent-ion conditions but is extended to lifetimes of up to ∼1 s under multi-axial tension.[43] This represents a greater than 12-fold increase in transition state lifetime, enabling the first direct single-molecule characterization of this elusive intermediate under physiologically relevant buffer conditions containing 12.5 mM Mg^{2+}. Our confidence in identifying these transition states stems from the robustness of the BNP-FRET approach, which explicitly accounts for camera noise and background fluctuations, allowing us to distinguish genuine intermediate states from the experimental artifacts.[38,44,45] Unlike random noise, which persists for only 1—2 time bins (40 ms each), the observed transition states persist significantly longer and occur repeatedly across multiple trajectories, confirming their physical and biological relevance, especially in facilitating the kinetic class interconversion.

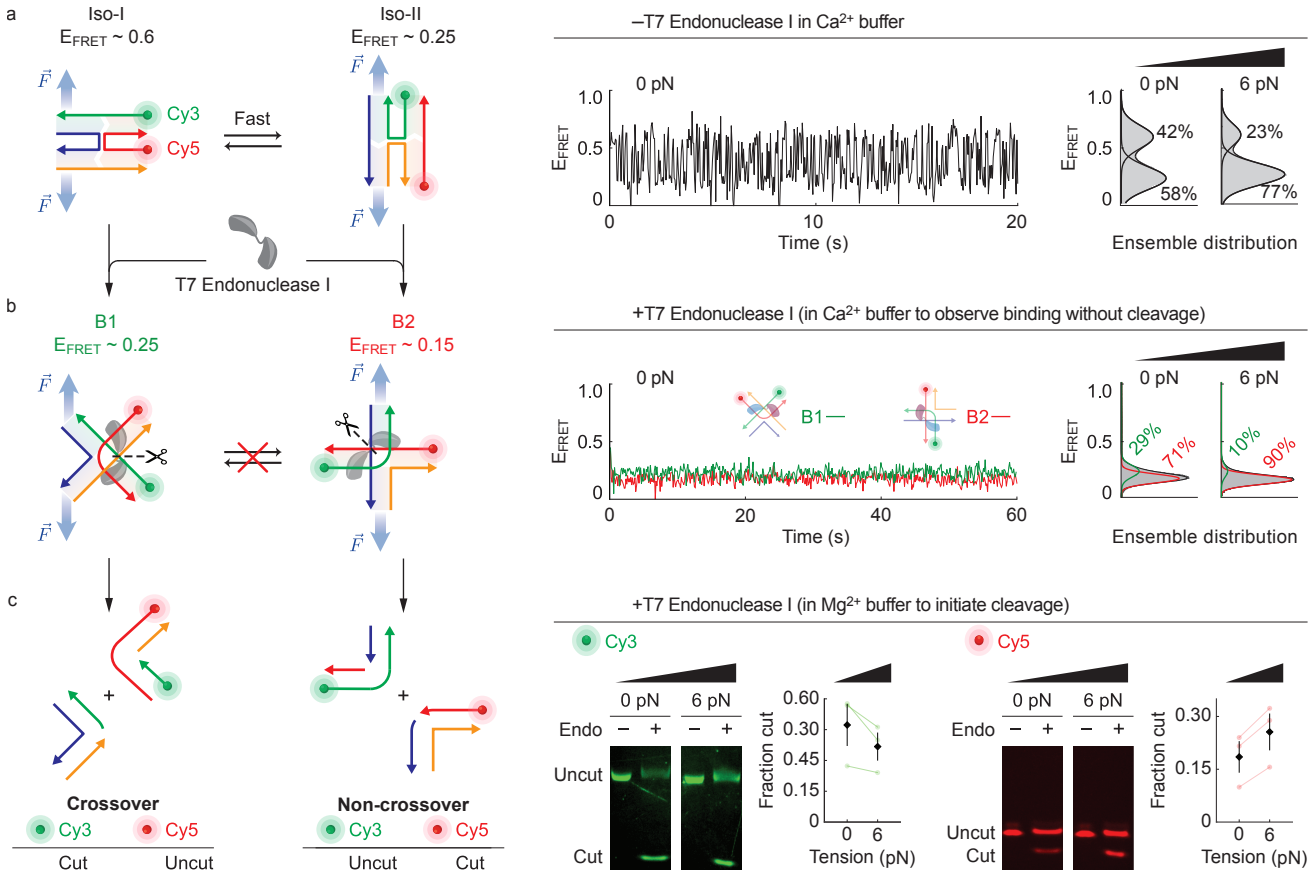

Fig. 5 Mechanical tension tunes Holliday junction resolution into crossover and non-crossover products under T7 Endonuclease I. (**a**) Baseline HJ dynamics under single-axial tension in Ca^{2+} buffer. Schematics show HJ isomers (Iso-I and Iso-II) under an applied force ($\vec{F}$) with FRET pair labeling (Cy3/Cy5, left). Representative smFRET trace indicates conformational dynamics in Ca^{2+} buffer without enzyme (middle). Ensemble FRET distributions at 0 pN and 6 pN tension show population shifts (N >140, right). (**b**) Enzyme-binding conformations under tension in Ca^{2+} buffer (binding without cleavage). Schematics of T7 endonuclease I binding to HJ under force, showing two distinct bound states (B1: $E_{FRET} \sim 0.25$; B2: $E_{FRET} \sim 0.15$, left). Representative smFRET trace in Ca^{2+} buffer with the enzyme, revealing stable binding without cleavage (middle). Ensemble distributions demonstrate tension-dependent binding preferences (right). (**c**) Tension-directed resolution outcomes in Mg^{2+} buffer (enabling cleavage). Schematics show two possible cleavage pathways leading to crossover (Cy3 cut, Cy5 intact) or non-crossover (Cy3 intact, Cy5 cut) products (left). Denaturing PAGE analysis and quantification shows that 6 pN tension significantly altered the crossover/non-crossover ratio compared to 0 pN, demonstrating mechanical control of genetic recombination outcomes (N=3 independent experiments; error bars: SD, right).

Pico Newton forces regulate enzymatic reaction outcomes through control of enzyme-substrate conformations. We tested this enzymatic mechanoregulation hypothesis using T7 endonuclease I, a resolvase that cleaves HJs at specific sites to generate crossover or non-crossover products during DNA repair. Tension at 6 pN induced shifts in enzyme binding conformations (B1 and B2 states) in Mg^{2+} free buffer containing Ca^{2+}, which inhibits cleavage while preserving binding interactions (Fig. 5(a and b)), demonstrating force-dependent enzyme-substrate interactions. Separately, tension at 6 pN only reduced the enzyme's cleavage activity by ∼5% compared to tension-free conditions, as quantified by denaturing PAGE analysis of Cy3/Cy5-labeled DNA strands (Fig. 5(c)). Despite the modest reduction in the overall cleavage rate, tension selectively altered cleavage patterns, increasing Cy5-strand cleavage while decreasing Cy3-strand cleavage, demonstrating that forces bias resolution toward specific crossover outcomes rather than simply reducing overall activity. This substantial modulation of enzymatic function directly links the conformational stabilization effects observed in our single-molecule studies to biologically relevant outcomes, demonstrating that single-axial forces can bias DNA repair pathways by mechanically modulating enzyme-substrate interactions. The magnitude of this effect suggests that cellular force environments may play a previously unrecognized role in regulating the balance between crossover and non-crossover repair outcomes during homologous recombination.

Discussion

MAESTRO represents a significant advance in single-molecule force spectroscopy by enabling programmable multi-axial tension application through a rigid DNA origami scaffold. In contrast to conventional techniques, which are limited to single-axis forces, MAESTRO uses ssDNA entropic springs anchored to a symmetric ring structure to generate physiologically relevant multi-directional force environments spanning 0–9 pN from up to four directions. This capability revealed previously undetectable HJ dynamics, including 5-fold kinetic slowing, stabilization of intermediate states with lifetimes up to ∼1 s, and kinetic class interconversion within individual molecules, which remained inaccessible to single-axis methods despite their proven value in mechanobiology research. These discoveries challenge the conventional understanding that increased mechanical force universally accelerates molecular dynamics, while acknowledging that MAESTRO's current force range and temporal resolution may limit its applications to faster dynamics or higher-force processes.

Multi-axial tension accesses expanded conformational landscapes by stabilizing transition states through mechanisms distinct from single-axis force applications. We discovered that 4-way tension slows HJ kinetics by over 5-fold while allowing quasi-ergodicity through kinetic class interconversion, demonstrating that physiological force environments create kinetic traps through multi-directional stress patterns rather than simple force magnitude effects. The stabilized intermediate state at E_{FRET}∼0.45—representing the open conformation that mediates isomer transitions—persists for up to 1 s under 4-way tension compared to <80 ms under tension-free conditions. This dramatic lifetime extension reveals how multi-directional forces can transform transient intermediates into stable, observable states by creating isotropic stress environments that favor symmetric conformations over the asymmetric stacking arrangements preferred under unidirectional tension.

The mechanistic basis for these expanded conformational landscapes involves alterations to the internal multiloop topology of the HJ at the crossover point, analogous to the way divalent cations modulate junction dynamics through electrostatic stabilization.[46,47] Multi-directional tension facilitates rearrangement of loop-forming sequences near the junction core by applying symmetric stress that stabilizes the open conformation, potentially through the release of trapped Mg^{2+} ions that otherwise lock the junction in specific conformational states, creating a more complex energy landscape with multiple intermediate states and alternative transition pathways. This mechanism explains both the dramatic kinetic slowing, as multi-axial forces create energetic barriers that trap the junction in long-lived conformations, and the emergence of kinetic class interconversion, as the expanded conformational space enables transitions between previously isolated dynamic regimes. The correlation between force directionality and kinetic

effects supports this model: while single-axis forces bias the junction toward specific stacked conformations through asymmetric stress, multi-axial forces create isotropic stress environments that preferentially stabilize the symmetric, open state.

This conformational control mechanism extends beyond HJs to establish a direct link between the cellular force environment and enzymatic regulation. The force-dependent nicking positions of T7 endonuclease I activity result from the stabilization of HJ conformations that are less favorable for enzyme binding and catalysis, demonstrating how multi-axial forces can bias DNA repair pathways through substrate conformational selection. This principle of force-dependent conformational control has broad implications for mechanobiology, including tension-dependent integrin activation in focal adhesions[24], force-regulated polymerase activity during transcription[16], and mechanosensitive ion channel gating, all of which rely on similar mechanisms in which mechanical forces bias protein conformations to modulate function. However, our findings suggest that multi-axial forces may be particularly important in cellular contexts requiring precise regulatory control, as they provide access to conformational states and kinetic regimes that are unavailable to simpler force patterns, potentially explaining why cells have evolved complex multi-directional force networks. The quasi-ergodicity achieved by multi-axial forces provides a fundamental mechanism for regulating cellular functions, where complex force networks could serve as molecular switches that control whether biomolecules remain trapped in specific functional states or can dynamically sample their full conformational space.

Building on these mechanistic insights, MAESTRO enables the investigation of biomolecular systems that experience complex force environments in their native cellular contexts while acknowledging current technical limitations. The platform is immediately applicable to mechanosensitive proteins, including ion channels that experience membrane tension from multiple directions, integrins that simultaneously experience forces from the extracellular matrix and cytoskeletal networks, and intrinsically disordered proteins that may adopt different conformations under multi-directional stress. Current constraints include the 0–9 pN force range, which may miss higher-force processes, and ms temporal resolution, which limits the detection of faster dynamics. Near-term technical developments should focus on extending the force range through shorter entropic springs (targeting 10–50 pN), improving temporal resolution through single-photon detection systems (targeting μs timescales), and developing asymmetric force patterns to recreate specific cellular stress environments. These enhancements will establish MAESTRO as an essential tool for understanding how physiological multi-axial forces regulate cellular function, while the current platform already provides unprecedented access to multi-directional force effects that have remained hidden from conventional single-molecule approaches.

Funding

The research was funded by the National Institutes of Health (NIH) (1DP2AI144247) and the National Science Foundation (NSF) through NSF CAREER (MCB 2341002) to R.F. Hariadi. S. Presse acknowledges support from the NIH (R01GM134426, R01GM130745, R35GM148237), US Army (ARO) (W911NF-23-1-0304) and NSF (2310610). G. B. M. Wisna was supported by an American Heart Association (AHA) predoctoral fellowship (23PRE1029870).

Acknowledgements

The authors gratefully acknowledge Chenxiang Lin for providing the Cadnano file of the NuPOD ring, for valuable scientific discussions, and for suggesting the T7 endonuclease I enzymatic assays. We acknowledge the use of facilities within the Eyring Materials Center and computational resources from the Phoenix and Sol supercomputers at Arizona State University.

Author Contributions

G.B.M.W. and R.F.H. conceived the idea for the study. G.B.M.W., R.S., D.K., and P.C. assisted with the experiments. G.B.M.W., A.S., and R.F.H. performed the analyses. G.B.M.W., A.S., D.K., P.C., S.P.,

and R.F.H. assisted with manuscript editing. All authors discussed the results and commented on the manuscript.

Correspondence

All correspondence and requests for materials should be addressed to G.B.M. Wisna and R.F. Hariadi.

References

1. Phillips R, Kondev J, Theriot J, Garcia H (2012) *Physical biology of the cell.* (Garland Science).
2. Bustamante C, Chemla YR, Forde NR, Izhaky D (2021) Optical tweezers in single-molecule biophysics. *Nat. Rev. Methods Primers* 1:25.
3. Tapia-Rojo R, Alonso-Caballero A, Fernandez JM (2024) Single-molecule force spectroscopy and molecular dynamics simulations reveal the mechanical stability of the C-terminal domain of SARS-CoV-2 nucleocapsid protein. *Nat. Commun.* 15:1564.
4. Rief M, Pascual J, Saraste M, Gaub HE (1997) Single molecule force spectroscopy of spectrin repeats: low unfolding forces in helix bundles. *J. Mol. Biol.* 286:553.
5. Yang D, Ward A, Halvorsen K, Wong WP (2016) Multiplexed single-molecule force spectroscopy using a centrifuge. *Nat. Commun.* 7:11026.
6. Zhang DY, Hariadi RF, Choi HM, Winfree E (2014) DNA origami-based force sensors for single-molecule force spectroscopy. *Nat. Nanotechnol.* 9:1024.
7. Wang X, Ha T (2013) Defining single molecular forces required to activate integrin and notch signaling. *Science* 340:991.
8. Jo MH, Cottle WT, Ha T (2024) Determination of single-molecule loading rate during mechanotransduction in cell adhesion. *Science* 383:1374.
9. Jo MH, Menon AK, Wollmuth LP, Ha T (2022) Single-molecule characterization of the dynamics of calmodulin bound to calcium channels. *Nat. Commun.* 13:7841.
10. Choi B, Zocchi G, Wu Y, Chan S, Jeanne Perry L (2005) Allosteric control through mechanical tension. *Phys. Rev. Lett.* 95(7):078102.
11. Nickels PC, et al. (2016) Molecular force spectroscopy with a DNA origami-based nanoscopic force clamp. *Science* 354:305.
12. Hellenkamp B, et al. (2018) Precision and accuracy of single-molecule FRET measurements—a multi-laboratory benchmark study. *Nat. Methods* 15:669.
13. Yasuda R, Noji H, Kinosita Jr K, Yoshida M (1998) F1-ATPase is a highly efficient molecular motor that rotates with discrete 120° steps. *Cell* 93:1117.
14. Altman RB, et al. (2004) The mechanism of ATP synthase. *Cell* 118:419.
15. Svoboda K, Block SM (1994) Force and velocity measured for single kinesin molecules. *Cell* 77:773.
16. Wuite GJ, Smith SB, Young M, Keller D, Bustamante C (2000) Single-molecule studies of the effect of template tension on T7 DNA polymerase activity. *Nature* 404:103.
17. Abraham A, et al. (2023) High-throughput single-molecule experiments reveal heterogeneity, state switching, and three interconnected pause states in transcription. *Cell Res.* 33:220.
18. Hohng S, et al. (2007) Fluorescence-force spectroscopy maps two-dimensional reaction landscape of the holliday junction. *Science* 318:279.
19. Yu H, Siewny MG, Edwards DT, Sanders AW, Perkins TT (2017) Hidden dynamics in the unfolding of individual bacteriorhodopsin proteins. *Nature* 543:265.
20. Bustamante CJ, Chemla YR, Liu S, Wang MD (2020) Single-molecule studies of protein folding with optical tweezers. *Annu. Rev. Biochem.* 89:443.
21. Neuman KC, Nagy A (2008) Single-molecule force spectroscopy: optical tweezers, magnetic tweezers and atomic force microscopy. *Nat. Methods* 5:491.
22. Dulin D, et al. (2015) High spatiotemporal-resolution magnetic tweezers: calibration and applications for DNA dynamics. *Biophys. J.* 109:2113.
23. Moffitt JR, Chemla YR, Smith SB, Bustamante C (2008) Recent advances in optical tweezers. *Annu. Rev. Biochem.* 77:205.
24. Geiger B, Spatz JP, Bershadsky AD (2009) Environmental sensing through focal adhesions. *Nat. Rev. Mol. Cell Biol.* 10:21.
25. Giancotti FG, Ruoslahti E (1999) Integrin signaling. *Science* 285:1028.

26. Haber JE (2018) DNA repair: the search for homology. *Bioessays* 40(5):1700229.
27. Rothemund PW (2006) Folding DNA to create nanoscale shapes and patterns. *Nature* 440:297.
28. Dietz H, Douglas SM, Shih WM (2009) Folding DNA into twisted and curved nanoscale shapes. *Science* 325:725.
29. Smith SB, Cui Y, Bustamante C (1996) Overstretching B-form DNA: the elastic response of individual double-stranded and single-stranded DNA molecules. *Science* 271:795.
30. Fisher PD, et al. (2018) Programmable assembly of DNA origami arrays. *Nature* 562:1508.
31. Hadden JM, Declais AC, Phillips SE, Lilley DM (2007) Structural basis of Holliday junction resolution by T4 endonuclease VII. *Nature* 449:621.
32. Ortiz-Lombardia M, et al. (1999) Crystal structure of a junction between B-DNA and Z-DNA reveals two extruded bases. *Nature* 399:396.
33. Zhou R, et al. (2019) Junction resolving enzymes use multimery to keep the Holliday junction dynamic. *Nat. Chem. Biol.* 15:269.
34. Biertümpfel C, Yang W, Suck D (2007) Crystal structure of T4 endonuclease VII resolving a Holliday junction. *Nature* 449:616.
35. Declais AC, Liu J, Freeman AD, Lilley DM (2003) The complex between a four-way DNA junction and T7 endonuclease I. *EMBO J.* 22:1398.
36. Wyatt HD, West SC (2014) Holliday junction processing activity of the Escherichia coli RuvABC nuclease. *Cold Spring Harb. Perspect. Biol.* 6:a023192.
37. Nettels D, et al. (2024) Single-molecule FRET for probing nanoscale biomolecular dynamics. *Nat. Rev. Phys.* 6:587.
38. Saurabh A, Wisna GBM, Schwieger M, Hariadi RF, Pressé S (2025) Bayesian nonparametrics for FRET using realistic integrative detectors. *BioRχiv.* https://www.biorxiv.org/content/10.1101/2025.06.12.659382v1.
39. Schnitzbauer J, Strauss MT, Schlichthaerle T, Schueder F, Jungmann R (2017) Super-resolution microscopy with DNA-PAINT. *Nat. Protoc.* 12:1198.
40. Hart DJ, Tamulaitis G, Siksnys V, Halford SE, Szczelkun MD (2023) Weak DNA binding and strong terminal base-pair recognition by the Holliday junction resolvase RuvC. *Nucleic Acids Res.* 51:3030.
41. Jungmann R, et al. (2010) Single-molecule kinetics and super-resolution microscopy by fluorescence imaging of transient binding on DNA origami. *Nano Lett.* 10:4756.
42. Hyeon C, Lee J, Yoon J, Hohng S, Thirumalai D (2012) Hidden complexity in the isomerization dynamics of Holliday junctions. *Nat. Chem.* 8:651.
43. Joo C, Balci H, Ishitsuka Y, Buranachai C, Ha T (2004) Exploring protein folding energy landscape by single-molecule fluorescence spectroscopy. *Annu. Rev. Biochem.* 73:739.
44. Saurabh A, Fazel M, Presse S (2023) Single-molecule FRET for probing nanoscale biomolecular dynamics. *Biophys. Rep.* 3.
45. Saurabh A, Fazel M, Presse S (2023) Single-molecule FRET for probing nanoscale biomolecular dynamics. *Biophys. Rep.* 3.
46. McKinney SA, Declais AC, Lilley DM, Ha T (2003) Structural dynamics of individual Holliday junctions. *Nat. Struct. Biol.* 10:93.
47. Lilley DM (2000) Structures of helical junctions in nucleic acids. *Q. Rev. Biophys.* 33:109.
48. Zadeh JN, et al. (2011) NUPACK: analysis and design of nucleic acid systems. *J. Comput. Chem.* 32:170.
49. Kapanidis AN, et al. (2004) Fluorescence-aided molecule sorting: analysis of structure and interactions by alternating-laser excitation of single molecules. *Proc. Natl. Acad. Sci. U. S. A.* 101:8936.

Materials and methods

Materials. Unmodified and biotinylated DNA staple strands for DNA origami MAESTRO were purchased from Integrated DNA Technologies (IDT Coralville, IA, USA). Scaffold strands (p8064) were sourced from Bayou Biolabs (Metairie, LA, USA). Amine-modified DNA strands used as imager strands were also obtained from IDT. Cy3B-NHS ester fluorophores (PA63101) were purchased from GE Healthcare (Chicago IL, USA). T7 endonuclease I (M0302L) was obtained from New England Biolabs (Ipswich, MA). BSA-biotin (A8549) and streptavidin (S4762) were purchased from Sigma-Aldrich (St. Louis, MO). All general chemicals were supplied by Sigma-Aldrich, unless otherwise noted. Glass coverslips (48466-205, 24×60 mm, #1.5) and microscope slides (16004-430) were obtained from VWR (Radnor, PA). Kapton tape (PPTDE-2, 0.5 mm thickness) was acquired from Bertech (Skokie, IL, USA). Amicon Ultra-0.5 centrifugal filter units (100 kDa MWCO, UFC510024) were purchased from Millipore Sigma. Carbon-coated TEM

grids (01814-F) were purchased from Ted Pella (Redding, CA, USA). Uranyl acetate and all buffer components were obtained from Sigma-Aldrich.

DNA-PAINT Imager Strands. Imager strands (TATGTAGATC/3' Cy3B/) were prepared by conjugating amine-modified DNA oligonucleotides with Cy3B fluorophores via NHS ester coupling. The conjugated products were subsequently purified using high-performance liquid chromatography (HPLC).

Tension Force Estimation Using the Modified Freely-Jointed Chain (FJC) Model. We estimated the tension force generated along the ssDNA springs using a modified freely-jointed chain (FJC) polymer model (Eq. 1).[29]

$$d = L_{ss}\left[\coth\left(\frac{FL_K}{k_BT}\right) - \frac{k_BT}{FL_K}\right]\left(1+\frac{F}{S}\right), \qquad [1]$$

where d is the end-to-end distance of the ssDNA spring (45 nm for MAESTRO), $L_{ss} = N \cdot l_{nt}$ is the total contour length with N nucleotides and $l_{nt} = 0.6$–0.7 nm per nucleotide, F is the applied tension, $L_K = 1.5$ nm is the Kuhn length, and S is the elastic modulus.[29]

To achieve the desired tension values, the selected staple strands were extended with uniquely designed ssDNA spring sequences at defined positions (Table S1). Spring sequences were designed using NUPACK[48] to minimize the self- and cross-interactions between springs, ensuring consistency with the FJC model assumptions of non-interacting polymer chains (Fig. S9).

MAESTRO Folding and Purification. DNA origami MAESTRO structures were assembled by mixing p8064 scaffold strands (20 nM final concentration) with staple strands, biotinylated strands, and entropic spring strands (each at 200 nM, 10-fold molar excess) in folding buffer (1× TAE, 12.5 mM $MgCl_2$, pH 8.0). Total reaction volume was 50 µL (Tables S1 and S4). The annealing protocol consisted of: (1) initial denaturation at 80 °C for 5 min, (2) gradual cooling to 4 °C at 0.31 °C/min (3 min 12 s per degree), and (3) storage at 4 °C until use. Folded structures were purified by 5 rounds of centrifugal filtration (Amicon Ultra-0.5, 100 kDa MWCO) at 14,000×g for 10 min each, with buffer exchange to storage buffer (1× TAE, 12.5 mM $MgCl_2$).

Negative-Stain Transmission Electron Microscopy of MAESTRO. Amicon-purified MAESTRO samples were diluted to a final concentration of 2 nM in 1× TAE buffer supplemented with 12.5 mM $MgCl_2$. Carbon-coated TEM grids (Ted Pella 01814-F) were glow-discharged for 30–60 s prior to sample application using a PELCO easiGlow glow discharge cleaning system. A 10 µL aliquot of the diluted sample was applied to the grid and incubated for 1–2 min at room temperature. Excess liquid was gently wicked off using a Whatman filter paper without allowing the grid to dry completely. For negative staining, 10 µL of 2% (w/v) aqueous uranyl acetate solution containing 25 mM NaOH was applied and immediately wicked away. A second 10 µL aliquot of the same staining solution was added and incubated on the grid for 30–60 s before removal. The grids were then completely air-dried before imaging.

Negatively stained samples were imaged using a Talos L120C G2 transmission electron microscope (Thermo Fisher Scientific) operated at 120 kV with a magnification of 57,000×. Images were acquired using a Ceta 16M camera, and pixel size calibration was performed using a standard calibration grid.

Holliday Junction (HJ) Formation. HJ samples were prepared by mixing four single-stranded DNA (ssDNA) oligonucleotides at equimolar concentrations. Specific strand extensions were included in the selected strands depending on the desired tension configuration (two-way, three-way, or four-way; see Table S2). The strands were diluted in buffer to a final concentration of 1× TAE supplemented with 12.5 mM $MgCl_2$. The mixture was annealed by heating to 80 °C for 5 mins, followed by gradual cooling to 4 °C at a rate of 3 mins and 12 secs per degree Celsius.

DNA-PAINT Super-Resolution Imaging for Short Oligo Tension Studies and Data Processing. MAESTRO structures bearing different ssDNA entropic springs corresponding to defined tension values were folded and purified as described above. These were then mixed with short docking oligos at equimolar concentrations and incubated at room temperature for ≥3 h to allow hybridization of the docking strands (Table S1) to the ssDNA springs (spring-1 and spring-2).

DNA-PAINT super-resolution imaging was performed following established protocols.[39] MAESTRO structures bearing 8 docking sites on their inner sidewalls (Fig. 1e, right panel and Fig. S2) or incorporating short oligos under defined mechanical tension (Fig. 1g, left panel; Tables S3 and S4) were immobilized onto coverslips coated with BSA-biotin and streptavidin. Coverslips were assembled into flow chambers using standard glass microscope slides and double-sided Kapton tape (0.5 mm thickness). For surface preparation, BSA-biotin and streptavidin were diluted to final concentrations of 1 mg/mL and 0.5 mg/mL, respectively, in Buffer A+ (10 mM Tris-HCl, 100 mM NaCl, 0.05% (v/v) Tween 20, pH 8.0).

MAESTRO samples were diluted to 2 nM in Buffer B+ (5 mM Tris-HCl, 12.5 mM $MgCl_2$, 1 mM EDTA, 0.05% (v/v) Tween 20, pH 8.0). The final imaging buffer contained an oxygen scavenging system comprising 1.25× PCA, 1× PCD, and 1× Trolox, along with 5 nM imager strands (TATGTAGATC/3' Cy3B/). Flow chambers were sealed with epoxy before imaging.

Imaging was conducted using an Oxford Nanoimager (ONI) Benchtop Nanoimager S Mark II equipped with total internal reflection fluorescence (TIRF) microscopy. Cy3B fluorophores were excited with a 532 nm laser at power densities between 800 and 1250 W/cm^2, and emission was collected using a 549–623 nm bandpass filter. A 100× oil-immersion Olympus objective (NA 1.49) was used, and images were captured with a Hamamatsu ORCA-Flash4.0 V3 sCMOS camera at exposure times of 200 ms per frame for MAESTRO constructs with eight docking sites and 100 ms for short oligos under tension studies. The system features z-lock autofocus and a piezo-controlled stage for precise positioning. All data were collected at room temperature (23 °C).

DNA-PAINT movies of MAESTRO constructs with eight docking sites were analyzed using Picasso software[39] for localization, rendering, and generation of averaged images from 412 MAESTRO molecules. Binding and unbinding durations were extracted from image stacks using a custom Python script. To estimate λ_{on} and λ_{off}, the distributions of the bright and dark times were fitted using the cumulative distribution function (CDF) of an exponential distribution (Fig. S3):

$$\text{CDF}(t) = 1 - \exp(-\lambda t) \qquad [2]$$

To analyze the force dependence of the oligo binding kinetics, we fitted the experimental data using the models from Hart et al.[40], given by:

$$k_{\text{off}}(F) = k_{\text{off}}(0) \exp\left[\frac{F \Delta x_{\text{off}}}{k_B T}\right], \qquad [3]$$

$$k_{\text{on}}(F) = k_{\text{on}}(0) \exp\left[\frac{\int_0^F \left(\frac{f}{a} + b\right) df}{k_B T}\right], \qquad [4]$$

where k_B is the Boltzmann constant, and T is the temperature. Parameters $k_{\text{off}}(0)$ and $k_{\text{on}}(0)$ represent the dissociation and association rates at $F = 0$ pN, respectively. Δx_{off} denotes the extension difference between the transition and bound states. Parameters a and b represent the differences in the stiffness and relaxed extension between the unbound and transition states. Fitted parameter values are summarized in Table S5.

smFRET of HJs Under Tension. MAESTRO constructs incorporating various single-stranded DNA (ssDNA) entropic springs, which were designed to generate specific tension magnitudes and configurations, were folded and purified. Corresponding HJ samples for each tension configuration were prepared separately. MAESTRO and HJ samples were then mixed in equal volumes to achieve a final concentration

of 5 nM each and incubated at room temperature on a shaker (400 rpm) for at least 4 hours to allow hybridization between the HJ extensions and the ssDNA springs.

smFRET samples were prepared on a coverslip assembled into a flow chamber using a glass microscope slide and double-sided Kapton tape. Surface functionalization was performed by sequentially introducing BSA-biotin and streptavidin, diluted to final concentrations of 1 mg/mL and 0.5 mg/mL, respectively, in Buffer A+ (10 mM Tris-HCl, 100 mM NaCl, 0.05% (v/v) Tween 20, pH 8.0). The MAESTRO–HJ complex was diluted to 2 nM in Buffer B+ (5 mM Tris-HCl, 12.5 mM $MgCl_2$, 1 mM EDTA, 0.05% (v/v) Tween 20, pH 8.0) and immobilized onto the functionalized coverslip.

Sample introduction into the flow chamber followed this sequence: 20 μL of BSA-biotin, a Buffer A+ wash, streptavidin, a second Buffer A+ wash followed by Buffer B+, the MAESTRO–HJ complex, a final Buffer B+ wash, and then the imaging buffer. Each step was incubated for 2 mins. The imaging buffer consisted of Buffer B+ supplemented with an oxygen-scavenging system containing 1.25× PCA, 1× PCD, and 1× Trolox. The flow chamber was sealed with epoxy prior to imaging.

smFRET imaging was performed using an Oxford Nanoimager (ONI) Benchtop Nanoimager S Mark II equipped with total internal reflection fluorescence (TIRF) optics. Alternating laser excitation (ALEX) was used to sequentially excite green (532 nm) and red (638 nm) lasers, which were synchronized with camera acquisition. Each excitation had a 20 ms exposure time, resulting in an effective binning time of 40 ms. A total of 5,000 frames were acquired for each field of view. Imaging was conducted using a 100× oil-immersion Olympus objective (NA 1.49), and fluorescence was captured with a Hamamatsu ORCA-Flash4.0 V3 sCMOS camera. Green laser power densities ranged from 115–340 W/cm^2, while red laser power ranged from 75–240 W/cm^2. The microscope was equipped with a z-lock autofocus system and piezo-controlled stage for high-precision imaging. All data were collected at room temperature (23 °C).

smFRET of HJs Under Tension with T7 endonuclease I. The preparation of MAESTRO–HJ samples followed the same protocol described in the smFRET of HJs Under Tension section, with one key modification: all buffers were prepared using 1× TAE containing 50 mM NaCl and 12.5 mM $CaCl_2$ instead of $MgCl_2$ to prevent cleavage of HJs by T7 endonuclease I.[33] A final concentration of 2 nM MAESTRO–HJ complex was mixed with T7 endonuclease I (New England Biolabs, catalog no. M0302L) at a final amount of 50 units (22.5 ng) in a 20 μL total reaction volume, yielding an enzyme concentration of approximately 18.7 nM. The mixture was incubated at room temperature for at least 10 mins to allow the enzyme to bind to the HJs prior to sample introduction into the flow chamber.

Flow chamber preparation and flow steps followed the same procedure as described in the smFRET of HJs Under Tension section, with buffer B+ replaced with C+ containing 10 mM Tris-HCl, 50 mM NaCl, 12.5 mM $CaCl_2$, 0.05% (v/v) Tween 20, and containing buffers to prevent the cleavage.

The smFRET imaging protocol was identical to the standard method, with a slight modification of the camera exposure time. For control experiments without T7 endonuclease I (Fig. 5b, top panel), a 20 ms exposure per frame was used. For samples containing T7 endonuclease I, the exposure time was increased to 60 ms (Fig. 5b, bottom panel) to improve the signal-to-noise ratio and enhance the resolution between the B1 and B2 smFRET states. All data were collected at room temperature (23 °C).

HJ Resolution by T7 endonuclease I Assessed via Denaturing PAGE Gel. To investigate the cleavage activity of T7 endonuclease I on HJs under defined tension conditions, we performed an electrophoretic mobility shift assay using denaturing PAGE. A 12% polyacrylamide gel was prepared in the presence of 8 M urea. MAESTRO DNA origami constructs were prepared to apply two different levels of tension to the HJs: 0 pN (tension-free control) and 6 pN. HJs without MAESTRO were included as an additional control. All samples were tested in both the presence and absence of T7 endonuclease I.

For the digestion assay, approximately 100 nM of each DNA sample was pre-incubated with 50 Units of T7 endonuclease I in reaction buffer (10 mM Tris-HCl, 50 mM NaCl, 12.5 mM $CaCl_2$, pH 7.9) at room temperature for 15 min to allow efficient enzyme binding. The cleavage reaction was initiated by incubation

at 30 °C for 40 min. The reaction was quenched by the addition of 0.5 M EDTA (final concentration 50 mM).

To denature the cleaved DNA fragments, equal volumes of formamide loading buffer were added to each sample, followed by heating at 90°C for 10 min. The denatured samples were loaded onto the gel and electrophoresed at 150 V for 1 h in 1× TBE buffer. After electrophoresis, the gel was stained with SYBR Gold nucleic acid gel stain and imaged using an Azure 300 gel documentation system (Azure Biosystems). Band intensities were analyzed using a custom Mathematica script to quantify the ratio of cleaved DNA fragments to total DNA fragments. Cleavage efficiency was calculated as the percentage of substrate converted to product bands.

BNP-FRET Analysis We employed Bayesian non-parametric FRET (BNP-FRET) analysis[37,38] to extract kinetic parameters from smFRET trajectories with an unprecedented accuracy and statistical rigor. This advanced method implements an infinite-dimensional hidden Markov model (HMM) that automatically determines the optimal number of conformational states without prior assumptions, while using Markov chain Monte Carlo (MCMC) techniques to generate comprehensive statistical samples for state trajectories, transition rates, and E_{FRET}s. The approach incorporates a sophisticated noise model specifically calibrated for our sCMOS camera system, including pixel-by-pixel calibration maps that maximize the signal recovery from noisy single-molecule data. The resulting MCMC samples enable the generation of detailed heatmaps for escape rates λ (representing the sum of all transition rates departing from a given state) and transition density plots (Fig. 1(c and d)), while providing robust uncertainty estimates for all the extracted parameters.

For each experimental dataset, we analyzed a minimum of three fields of view, with each field containing at least 2,500 frames to ensure the statistical robustness of our findings. Single-molecule FRET traces were extracted from more than 100 individual molecules per condition, providing sufficient data for reliable statistical inferences. To maintain data quality, we applied stringent filtering criteria, including ALEX stoichiometry filtering[49] to confirm single-molecule behavior, assessment of total donor and acceptor fluorescence stability during donor excitation to identify photobleaching or blinking artifacts, and a minimum requirement of at least one observable FRET state transition per trace to ensure dynamic behavior. Camera calibration involved acquiring 2,500 dark noise frames under identical experimental conditions but without laser excitation or sample presence. The local background fluorescence was systematically subtracted during trace extraction. The filtered and calibrated single-molecule traces were subsequently processed through the BNP-FRET computational pipeline on Arizona State University's high-performance computing clusters Sol and Phoenix, with detailed methodology described in Saurabh et al.[38]

Code Availability The BNP-FRET analysis pipeline is available at: https://github.com/LabPresse/BNP-FRET-Binned.